This papers appears in Mechatronics, 2021.
https://doi.org/10.1016/j.mechatronics.2021.102639

Enhancing Kinematic Accuracy of Redundant Wheeled Mobile Manipulators via Adaptive Motion Planning

Hongjun Xing[a,b], Ali Torabi[b], Liang Ding[a,*], Haibo Gao[a], Weihua Li[a] and Mahdi Tavakoli[b,*]

[a]State Key Laboratory of Robotics and System, Harbin Institute of Technology, Harbin 150001, China
[b]Department of Electrical and Computer Engineering, University of Alberta, Edmonton T6G 1H9, Alberta, Canada

ARTICLE INFO

Keywords:
Wheeled mobile manipulator
kinematic accuracy
joint constraints
adaptive motion planning
redundancy resolution

ABSTRACT

An increasing demand for wheeled mobile manipulators (WMMs) in fields that require high precision tasks has introduced new requirements as far as their kinematic accuracy. A WMM consists of a manipulator mounted on a mobile base. This configuration usually makes the WMM a redundant robotic system. One limiting factor is that the kinematic accuracy of the mobile base is often lower than that of the manipulator because of modelling errors and disturbances such as slippage. Thus, it makes sense to distribute more of a given set of motion requirements for the entire mobile manipulator to the manipulator when possible – this is usually done using a weighting matrix that sums the mobile base motion and the manipulator motion. In this paper, considering a redundant WMM, a novel adaptive motion planning method is proposed as a secondary objective in the null space of the primary objective (improvement of the WMM's kinematic accuracy) for the WMM. Also, a tertiary objective to move the manipulator away from its singularity is proposed. This objective is activated if the secondary objective is feasible and the WMM still has remaining redundant degrees of freedom. The proposed method is implemented at the acceleration level to circumvent the discontinuity of the commanded joint velocity due to the adaptive motion planning algorithm. The advantages and effectiveness of the proposed approach are demonstrated with a traditional motion planning approach through experiments.

1. Introduction

Wheeled mobile manipulators (WMMs) fuse the advantages of high mobility of a mobile base and dexterous operation ability of a manipulator. WMMs have been used in executing many tasks that need high precision, including door opening [1, 2], valve turning [3], object grasping [4, 5], and large-scale 3D printing [6]. The addition of a mobile base to a manipulator is an efficient method of extending the reach of the manipulator, which is otherwise restricted to a fixed workspace. This combination has presented new challenges to researchers. Due to the different characteristics of the base and the manipulator such as their kinematics and dynamics, the motion planning and control of the entire system (called the mobile manipulator) should take these differences into account [7]. Also, the combination of the mobile base and the manipulator often makes the WMM a kinematically redundant robotic system. A redundant robot has more degrees of freedom (DOFs) than minimally required for executing tasks. The inverse kinematics of any kinematically redundant robotic system admits an infinite number of solutions. Thus, redundancy makes it possible to have joint motions that do not affect the pose (position and orientation) of the end-effector[8, 9]. This inner joints motion can be used in closed-loop control to achieve a secondary objective while performing any primary objective, e.g., singularity avoidance, obstacle avoidance, manipulability enhancement, and/or force feedback capability maximization [10, 11, 12, 13].

The mobile base is often regarded as an extension to the manipulator, and the model of the entire system is established without considering the inherent differences between these two parts. For example, the base usually moves in an unstructured environment (e.g., slippage/skidding or locomotion on uneven ground) while the manipulator is in free or contact motion [14]. The kinematic accuracy of the mobile base is generally lower than that of the manipulator due to the unknown wheel-ground contact and the possibility of slippage. Thus, kinematic accuracy improvement of the WMM can be achieved by distributing more of the required motions to the manipulator than to the mobile base when the task permits.

Kinematic accuracy is of great importance for mobile robots, especially when they are working in constrained environments [15]. However, few studies were conducted to improve the kinematic accuracy of a WMM's end-effector with consideration of the motion errors of the mobile base. Shin *et al.* [16] improved the kinematic precision of a WMM by discretizing the task so that the mobile base and the manipulator did not move simultaneously. Papadopoulos *et al.* [17] presented a motion planning methodology for nonholonomic WMMs simultaneously following desired end-effector

*This work was supported by Canada Foundation for Innovation (CFI), the Natural Sciences and Engineering Research Council (NSERC) of Canada, the Canadian Institutes of Health Research (CIHR), the Alberta Advanced Education Ministry, the Alberta Economic Development, Trade and Tourism Ministry's grant to Centre for Autonomous Systems in Strengthening Future Communities, the National Natural Science Foundation of China (Grant No. 51822502, 91948202), the National Key Research and Development Program of China (No. SQ2019YFB130016), the Fundamental Research Funds for the Central Universities (Grant No. HIT.BRETIV201903), the "111" Project (Grant No. B07018), and the China Scholarship Council under Grant [2019]06120165.

*Corresponding authors
xinghj@hit.edu.cn (H. Xing); ali.torabi@ualberta.ca (A. Torabi); liangding@hit.edu.cn (L. Ding); gaohaibo@hit.edu.cn (H. Gao); liweihua@hit.edu.cn (W. Li); mahdi.tavakoli@ualberta.ca (M. Tavakoli)

and mobile base trajectories without violating the nonholonomic constraints, assuming that the base had no kinematic error. Nagatani *et al.* [18] presented a cooperative motion planning method for WMMs without considering the kinematic motion error of the mobile base. Jia *et al.* [7] paid attention to the differences between the mobile base and the manipulator. They proposed a coordinated motion planning method based on a weighted inverse Jacobian for nonholonomic mobile manipulators without considering the joint constraints (position, velocity, and acceleration). The employment of a weighted inverse Jacobian could realize motion distribution between the two sub-systems (the mobile base and the manipulator). Xing *et al.* [19] employed a weighting matrix to distribute the desired end-effector motion of an omnidirectional mobile manipulator to the movement of the mobile base and the action of the manipulator with consideration of the manipulator joint limits at the velocity level to improve the kinematic accuracy of the total system. Yet, this motion planning approach did not fully utilize the manipulator's redundancy [20] because when one of the manipulator's joint exceeded its limit, the motion requirement would simply be transferred to the mobile base.

The motion planning of redundant WMMs can also be formulated as an optimization problem with equality or inequality constraints[21, 22], such as quadratic programming (QP) problem [23]. The problem of the QP-based methods lies in two aspects. First is the high computational load when the number of DOFs rises, and second is the occurrence of the cases of multiple hierarchical tasks or impracticable tasks [24]. In order to solve the problem of multiple prioritized tasks, Kanoun *et al.* [25] presented a prioritized task-regulation framework, which covered both linear equalities and inequalities. For real-time implementation, Escande *et al.* [26] proposed a generic solution to solve multiple prioritized problems of both equality and inequality constraints, which was ten times faster than the iterative-projection hierarchical solvers when only equalities considered. Nevertheless, when hard joint constraints of the manipulator are taken into account, the QP-based approach cannot take the advantage of formulating all the inequalities in a unified framework [27]; thus, the computation complexity of these algorithms will be very high.

In this paper, a novel method to enhance the kinematic accuracy of redundant WMMs by adaptive motion planning with null-space implementation is proposed. As stated before, the kinematic accuracy of the mobile base is inferior to that of the manipulator. Therefore, the redundancy of the WMM can be employed to, first, assign all of the desired motion to the manipulator to execute. Next, when the manipulator reaches its limit (being joints' range, velocity, and/or acceleration limit) and the desired motion is not feasible for it anymore, the adaptive motion planning approach will be executed in the null space of the system. Consequently, some parts of the desired motion will be transferred to the mobile base to make the desired trajectory feasible for the WMM.

The proposed method builds upon the work by Flacco *et al.* [27] for redundant manipulators and extends it to redundant WMMs. The "saturation in the null-space" (SNS) algorithm proposed by Flacco *et al.* [27] handles the joint bounds of a redundant manipulator by successively discarding the joints that would exceed their motion bounds when using the minimum norm solution. The SNS method is excellent in addressing the redundant system's limitations due to its adequate and accurate distribution of end-effector's Cartesian motion to joint motion. However, this method has never been employed to enhance the kinematic accuracy of WMMs. With this in mind, we present an adaptive motion planning (AMP) method to enhance the kinematic accuracy of a WMM using its null space. This method passes the desired motion as much as possible to the manipulator via the null space of the WMM until the motion is not feasible for the manipulator. Then, the motion will be decomposed to a motion for the mobile base and a feasible motion for the manipulator. Furthermore, suppose after resolving all of the joint limits, the WMM has some redundancy left. In that case, a tertiary objective will be pursued in the null space of the secondary objective for the robotic system to avoid singularities. It is worth mentioning that the proposed method is implemented at the joint acceleration level to avoid velocity discontinuity when the mobile base is enabled/disabled.

In the proposed method, the singularity of the manipulator will first be examined. If the manipulator is close to a singular configuration, the mobile base will be activated at once. Thus, only when the manipulator is away from the singularity, will the motion planning approach be executed. Meanwhile, the tertiary objective will be performed to keep the manipulator from singularity without intervening with the primary and secondary tasks.

The remainder of this paper is organized as follows. The kinematic model and motion planning of the WMM is provided in Section 2. In Section 3, the proposed adaptive motion planning method is presented. In Section 4, experimental results are reported to examine the performance of the proposed motion planning strategy. Concluding remarks appear in Section 5.

2. Kinematic Modeling and Motion Planning of a Mobile Manipulator

The kinematics of a mobile manipulator can be obtained from the kinematic models of the two subsystems, i.e., the mobile base and the manipulator. As shown in Fig. 1, Σ_w, Σ_b, Σ_m, and Σ_{ee} are considered as the world reference frame, mobile base frame, manipulator reference frame, and end-effector frame, respectively. First, let us derive the kinematic model of the mobile base. Assume the contact between the wheels of the mobile base and the ground is pure rolling (i.e., no slippage). Then, its kinematic model can be obtained as

$$\dot{q}_b = P(q_b)v_b, \tag{1}$$

where $q_b \in \mathbb{R}^{n_b}$ denotes the generalized coordinate vector of the mobile base expressed in Σ_w, $v_b \in \mathbb{R}^b$ denotes the velocity vector of the wheels, $P(q_b) \in \mathbb{R}^{n_b \times b}$ denotes the constraint matrix of the base (holonomic or nonholonomic),

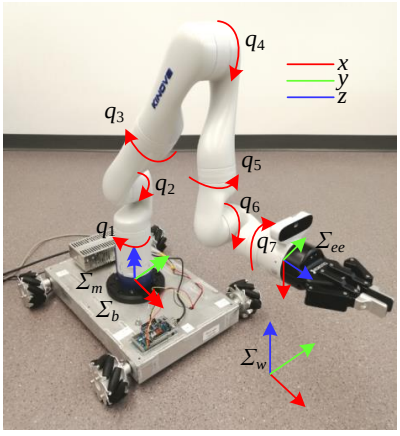

Figure 1: Omnidirectional wheeled mobile manipulator.

and n_b and b denote the dimensions of the generalized coordinate vector and the wheel velocity vector, respectively. $P(q_b)$ transfers the wheel velocities to the generalized base velocities. Also, it is worth mentioning that (1) is a generalized model, which is applicable to both holonomic and nonholonomic mobile bases.

Next, assume that the pose of the end-effector in Σ_w is defined as $x \in \mathbb{R}^r$, r is its dimension. The WMM's generalized coordinate vector denotes as $q = [q_b^{\mathrm{T}}, q_m^{\mathrm{T}}]^{\mathrm{T}} \in \mathbb{R}^n$, where $q_m \in \mathbb{R}^m$ is the generalized manipulator coordinate, m is its dimension (number of joints), and the subscript $n = n_b + m$. It is worth mentioning that the generalized manipulator velocity is defined as the velocity of the manipulator joints. Now, the WMM's forward kinematics at the velocity level can be calculated as [28]

$$\begin{aligned} \dot{x} = J(q)\dot{q} &= [J_b(q) \quad J_m(q)] \begin{bmatrix} \dot{q}_b \\ \dot{q}_m \end{bmatrix} \\ &= [J_b(q)P(q_b) \quad J_m(q)] \begin{bmatrix} v_b \\ \dot{q}_m \end{bmatrix} = J_v(q) \begin{bmatrix} v_b \\ \dot{q}_m \end{bmatrix}, \end{aligned} \tag{2}$$

where $J_b \in \mathbb{R}^{r\times n_b}$ is the Jacobian of the mobile base, $J_m \in \mathbb{R}^{r\times m}$ is the Jacobian of the manipulator, $J(q) \in \mathbb{R}^{r\times n}$ is the Jacobian of the generalized WMM (i.e., no constraints of the mobile base are considered), and $J_v(q) \in \mathbb{R}^{r\times(b+m)}$ is the Jacobian of the WMM. There are two Jacobians for a WMM, because the generalized coordinate of a mobile base is not its wheel velocity. It is worth noting that when the mobile base is subjected to nonholonomic constraints, only $J_v(q)$ can be employed. For a holonomic mobile base, both $J(q)$ and $J_v(q)$ can be utilized because they are equal to one another [29, 30].

The WMM is usually a kinematically redundant system (i.e., $r < n$). Thus, for a given task $\dot{x}$, all solutions $\dot{q}$ can be expressed as [31][1]

$$\dot{q} = J^{\dagger}\dot{x} + (I - J^{\dagger}J)\dot{q}_N, \tag{3}$$

[1]For brevity, the dependence of the Jacobian matrices upon the joint variables is omitted in the notation.

where $J^{\dagger} = J^{\mathrm{T}}(JJ^{\mathrm{T}})^{-1}$ is the pseudoinverse of J, I is an $n\times n$ identity matrix, $I - J^{\dagger}J$ is the null space of J, and $\dot{q}_N \in \mathbb{R}^n$ is the null-space velocity for sub-tasks. The derivative of (2) with respect to time derives

$$\ddot{x} = J\ddot{q} + \dot{J}\dot{q}. \tag{4}$$

Then, the WMM's kinematic model considering the null-space planning at the acceleration level can be expressed as

$$\ddot{q} = J^{\dagger}(\ddot{x} - \dot{J}\dot{q}) + (I - J^{\dagger}J)\ddot{q}_N. \tag{5}$$

3. Adaptive Motion Planning Method

The AMP method is proposed to improve a WMM's kinematic accuracy. With this method, the manipulator will completely undertake the task, and only when the range or acceleration requirements of the task exceed the limits of the manipulator, will the mobile base be involved.

3.1. Joint Acceleration Limits Definition

The motion of the WMM is planned at the acceleration level; therefore, the limits on joint acceleration need to be locally calculated. Taking into account the joint position, velocity and acceleration bounds of the WMM, its acceleration limits on $\ddot{q}$ at time $t = t_h$ can be expressed as [32]

$$\ddot{Q}_{\min}(t_h) \leqslant \ddot{q}(t_h) \leqslant \ddot{Q}_{\max}(t_h), \tag{6}$$

with the acceleration limits for each joint defined as

$$\ddot{Q}_{\min,i} = \begin{cases} \max\left\{ \dfrac{2(Q_{\min,i} - q_{h,i} - \dot{q}_{h,i}T)}{T^2}, \right. \\ \qquad \left. \dfrac{V_{\min,i} - \dot{q}_{h,i}}{T}, A_{\min,i} \right\}, & \text{if } q_{h,i} > Q_{low,i} \\ A_{\max,i}, & \text{else} \end{cases} \tag{7}$$

$$\ddot{Q}_{\max,i} = \begin{cases} \max\left\{ \dfrac{2(Q_{\max,i} - q_{h,i} - \dot{q}_{h,i}T)}{T^2}, \right. \\ \qquad \left. \dfrac{V_{\max,i} - \dot{q}_{h,i}}{T}, A_{\max,i} \right\}, & \text{if } q_{h,i} < Q_{up,i} \\ A_{\min,i}, & \text{else} \end{cases} \tag{8}$$

where $V_{\max}/V_{\min}$ and $A_{\max}/A_{\min}$ are the maximum and minimum hard joint bounds of the velocity and acceleration, respectively. $i = 1, \ldots, n$ denotes the i^{th} element of the corresponding vector, the sampling time is denoted as T, and $q_{h,i}$ denotes the current WMM joint position at time t_h of the i^{th} joint. $Q_{low,i}$ and $Q_{up,i}$ are defined as

$$Q_{low,i} = Q_{\min,i} - \frac{|\dot{q}_{h,i}|\,\dot{q}_{h,i}}{2A_{\max,i}},$$

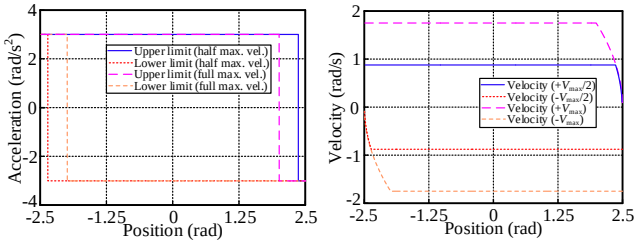

(a) Acceleration limit (b) Velocity profile

Figure 2: Joint acceleration limit and its corresponding velocity. $Q_{\max} = 2.5$ rad, $Q_{\min} = -2.5$ rad, $V_{\max} = 1.75$ rad/s, $V_{\min} = -1.75$ rad/s, $A_{\max} = 3$ rad/s^2, and $A_{\min} = -3$ rad/s^2.

$$Q_{up,i} = Q_{\max,i} + \frac{|\dot{q}_{h,i}|\,\dot{q}_{h,i}}{2A_{\min,i}}.$$

Fig. 2 presents a sample of joint acceleration limits and their corresponding joint velocities with given joint physical limits. In this example, the joint velocities are set as $V_{\max}/2$ and $V_{\max}$. As shown in Fig. 2, with the increase of the velocity, the acceleration change happens farther from the joint position bound. The joint needs more displacements to cease its motion at the physical limit due to the limited joint acceleration. Fig. 2b shows the corresponding velocity profile calculated according to the acceleration limit. With different velocities, the proposed acceleration limit calculation method can always make the joint velocity decrease to zero when the joint is close to the position bound. It should be noted that Fig. 2a shows the acceleration bounds of the joint, not its current acceleration.

3.2. Adaptive Motion Planning Framework

It is desirable to distribute the motion requirement of the end-effector as much as possible to the manipulator to have high motion accuracy. The AMP method makes use of the kinematic redundancy of the WMM to break down the desired motion between the mobile base and the manipulator. This method will distribute some of the motion to the mobile base only when the manipulator cannot handle the task by itself, i.e., one or more joints of the manipulator are at their limits or the manipulator is near a singular configuration.

In our previous work in [19], a weighting matrix was used to distribute the desired end-effector trajectory, which did not make the best use of the manipulator redundancy. Instead, in this paper, we propose the AMP method to fully utilize the manipulator's redundancy until it cannot execute the task. In the AMP method, first, a diagonal selection matrix $\mathcal{S}$ needs to be defined to specify the active joints. $\mathcal{S}$ is defined as an $n \times n$ diagonal selection matrix whose diagonal elements specify whether the joints are active or not, i.e., if the i element on the $\mathcal{S}$ diagonal is one, the i^{th} joint of the WMM is active. Then, by combining the selection matrix and (5), in the AMP method, the joint acceleration command is designed as

$$\ddot{q}_{amp} = (J\mathcal{S})^{\dagger}(\alpha\ddot{x} - \dot{J}\dot{q}) + [I - (J\mathcal{S})^{\dagger}J]\ddot{q}_N, \qquad (9)$$

where α is a scaling factor to downscale the Cartesian task $\ddot{x}$ when it is not feasible for the WMM. It is noteworthy that $\ddot{q}_N$ in (9) represents the null-space acceleration vector of the joints. If the i^{th} joint is not saturated, $\ddot{q}_{N,i} = 0$; else, $\ddot{q}_{N,i}$ is defined as the corresponding joint acceleration limit expressed in (6)-(8). More details are provided below.

Initially, the selection matrix is set to be $\mathcal{S} = \begin{bmatrix} 0_{n_b \times n_b}, & 0 \\ 0, & I_{m \times m} \end{bmatrix}$, i.e., the mobile base is deactivated and no motion will be distributed to the base (the null-space acceleration $\ddot{q}_N$ vector is set to be zero). Next, the joint acceleration command is calculated using (9). Here, if the i^{th} joint of the manipulator is over-driven (i.e., $\ddot{q}_{amp,i} > \ddot{Q}_{\max,i}$ or $\ddot{q}_{amp,i} < \ddot{Q}_{\min,i}$), the corresponding element on the $\mathcal{S}$ diagonal is chosen to be zero to disable the joint, and the i^{th} element of the null-space acceleration $\ddot{q}_N$ is set equal to $\ddot{Q}_{\max,i}$ or $\ddot{Q}_{\min,i}$. With this choice of $\ddot{q}_N$ and $\mathcal{S}$, the acceleration of the i^{th} joint will be adjusted back to its saturation level and the associated acceleration shortage will be assigned to the other joints of the manipulator. However, this may over-drive the other joints of the manipulator. Therefore, this method needs to be repeated iteratively until there is no over-driven joint left; otherwise, the Cartesian space acceleration $\ddot{x}$ is found to be infeasible for the WMM with the disabled mobile base.

The feasibility of the desired Cartesian acceleration can be inspected by checking the rank of $J\mathcal{S}$. If the rank of this matrix is smaller than the dimension of the Cartesian space r, the Cartesian space acceleration $\ddot{x}$ is not feasible for the manipulator. Thus, the mobile base needs to be activated by changing the corresponding elements of the selection matrix from zeros to ones. After activation of the mobile base, the joints' accelerations need to be adjusted again. If the desired Cartesian space acceleration is still infeasible for the WMM with the active mobile base, it has to be modified to become realizable for the WMM. In this case, we introduce a scaling factor $0 \leqslant \alpha \leqslant 1$ to make the desired Cartesian acceleration $\ddot{x}$ realizable. α is equal to one unless $\ddot{x}$ is not feasible for the WMM.

In experiments, we notice that using the above approach, the AMP method sometimes moves the manipulator to the edge of its workspace and then activates the mobile base. This causes workspace-boundary singularities as the manipulator is fully stretched out. Therefore, we add singularity avoidance to the proposed approach, which is performed in two stages. First, during each loop, the manipulator singularity is examined. If the current segment of the desired trajectory makes the manipulator approach its singularity, the mobile base is then activated. Second, a tertiary objective is utilized in the null-space planner that moves away the manipulator from singularity when it is possible. Here, we design the cost function inspired by the concept of velocity manipulability ellipsoid, which is an effective measure to evaluate the distance of a robotic system from its singularity [12]. For a manipulator, the ellipsoid is defined as $w(q_m) = \sqrt{\det(J_m J_m^{\mathrm{T}})}$. Instead of employing $w(q_m)$, we select the cost function as $H(q_m) = w^2(q_m) = \det(J_m J_m^{\mathrm{T}})$ to

make the optimization more computationally efficient. The computation of the partial derivative of H over q_m avoids the square root of det $(J_m J_m^{\mathrm{T}})$.

Prioritized task motion planning is an effective method that ensures the primary task gets completed. Then, if there is still redundancy remained, the sub-task (secondary task) will be executed [32]. Let us define the auxiliary null-space projection matrix in the joint space as

$$P_A = \left[I - \left((I - \mathcal{S}) P_N \right)^{\dagger} \right] P_N, \tag{10}$$

with $P_N = I - J^{\dagger} J$ being the orthogonal projector in the Jacobian null space. Now, the joints acceleration command corresponding to the tertiary objective can be designed as

$$\ddot{q}_t = \beta P_A \ddot{q}_A, \tag{11}$$

where $0 \leqslant \beta \leqslant 1$ is the scaling factor to preserve the joint bounds when the remained redundancy is not enough to handle it and $\ddot{q}_A$ is the joint acceleration vector associated with the null-space projection matrix P_A. The joint velocity for the tertiary objective (singularity avoidance) is defined as

$$\dot{q}_{SA} = \gamma_1 \begin{bmatrix} 0_{n_b \times 1} \\ (\nabla_{q_m} H)^{\mathrm{T}} \end{bmatrix}, \tag{12}$$

and then, the joint acceleration for this objective is designed as

$$\ddot{q}_A = \begin{bmatrix} 0_{n_b \times 1} \\ \gamma_1 (\nabla^2_{q_m} H) \dot{q}_m + \gamma_2 [\gamma_1 (\nabla_{q_m} H)^{\mathrm{T}} - \dot{q}_m] \end{bmatrix}, \tag{13}$$

in which γ_1 and γ_2 are two positive constants. The derivations of $\nabla_{q_m} H$ and $\nabla^2_{q_m} H$ are shown in Appendices A and B, respectively.

The joint acceleration command that realizes the above-mentioned desired Cartesian space acceleration, AMP method, and tertiary objective is

$$\ddot{q} = \ddot{q}_{amp} + \ddot{q}_t. \tag{14}$$

The flowchart of the motion planning system is shown in Fig. 3 and the method to determine the scaling factors α and β is illustrated in Fig. 4.

Fig. 3 presents the flowchart of the proposed motion planning method for a WMM with consideration of singularity avoidance. The primary task is to enhance the kinematic accuracy of the WMM via AMP (secondary task). Therefore, the mobile base is kept disabled until the manipulator joint is saturated or the manipulator is close to a singularity. A measure to detect the singular configuration is defined based on the minimum singular value of the manipulator Jacobian matrix J_m [33]. The minimum singular value is denoted as σ_m and the singularity measure is designated as $\sigma_{m,min}$. If $\sigma_m < \sigma_{m,min}$, which means that the singularity of the manipulator occurs, then, the mobile base will be activated to move the manipulator away from singularity. Also, when the system has remaining redundancy after the primary and secondary tasks are completed, the manipulator's ability

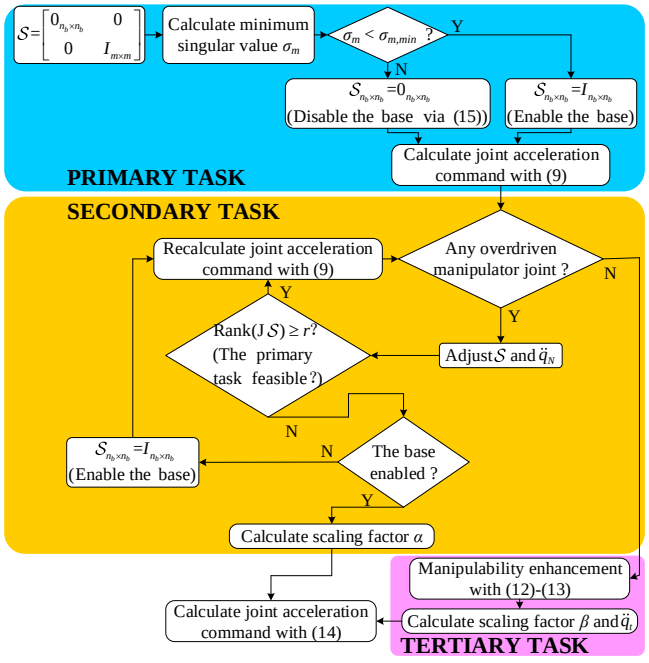

Figure 3: Flowchart of the motion planning for a WMM system.

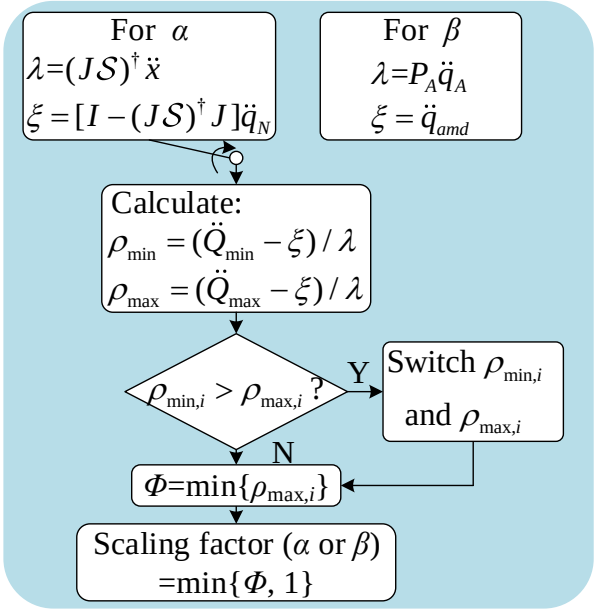

Figure 4: Flowchart of the scaling factor determination.

to stay away from singularity will be enhanced via the execution of the tertiary objective provided by (11). When the primary task or the tertiary task cannot be fully executed, a scaling factor α or β is added to downscale the task to make it partially completed.

With the motion planning approach executed at the acceleration level, once the mobile base is deactivated and without distributed acceleration, it will still move with a con-

stant velocity. However, our goal is to stop the mobile base smoothly to obtain a better WMM's kinematic accuracy when no acceleration is distributed to it. Here, a transition function is utilized to steadily cease the movement of the mobile base

$$\ddot{q}_{b,trans} = \begin{cases} \ddot{q}_b, & \text{if } t \leqslant t_0 \\ A_{\min,b}, & \text{if } sign(V_b) > 0 \ \& \ t_0 < t < t_f^+ \\ A_{\max,b}, & \text{if } sign(V_b) < 0 \ \& \ t_0 < t < t_f^- \\ 0, & \text{if } sign(V_b) > 0 \ \& \ t \geqslant t_f^+ \\ 0, & \text{if } sign(V_b) < 0 \ \& \ t \geqslant t_f^- \end{cases} \quad (15)$$

where $\ddot{q}_{b,trans}$ is the base acceleration during the transition process, t_0 and $t_f^+(t_f^-)$ represent the start and end time of the transition, respectively. Also, $t_f^+ = |\frac{V_b}{A_{\min,b}}| + t_0$ and $t_f^- = |\frac{V_b}{A_{\max,b}}| + t_0$. For the transition process, the mobile base will be deactivated with the maximum acceleration to keep high kinematic accuracy. V_b is the base velocity when it is deactivated and $\sigma_m \geqslant \sigma_{m,min}$ is achieved, and $A_{\max,b}$ and $A_{\min,b}$ are the maximum and minimum accelerations of the base, respectively.

Fig. 4 shows the process of determining the scaling factors according to the joint bounds (6)-(8). As shown in Fig. 4, λ denotes the required joint acceleration for the previous task, and ξ represents the consuming joint motion capability of the manipulator for the corresponding task. Then, we will calculate the ratio of the residual joint acceleration to the required joint acceleration (denoting as $\rho_{\min}$ and $\rho_{\max}$), and get the minimum ratio of all the joints, expressed as $\boldsymbol{\Phi}$. The parameter $\boldsymbol{\Phi}$ is a criterion indicating the residual capability of the manipulator to complete the task. If $\boldsymbol{\Phi} \geqslant 1$, the manipulator has enough capability to accomplish the task; if $\boldsymbol{\Phi} < 1$, the manipulator cannot fulfill the mission. Since we should not upscale the given task, the scaling factor (α or β) is chosen as the smaller one between $\boldsymbol{\Phi}$ and 1.

4. Experimental Results

In order to verify the effectiveness and advantages of the proposed AMP method, it was applied to a WMM and compared with a traditional motion planning approach that used the pseudoinverse of the Jacobian (we even extended the traditional approach to do manipulability enhancement). The experiments consist of three parts: (A) the verification of the importance of singularity avoidance, (B) and (C) the evaluation of the proposed motion planning method with end-effector's position and full pose considered, respectively.

4.1. Experimental Setup

The experiments were performed using an omnidirectional WMM. The WMM is the sum of a four-wheel mobile base and a 7-DOF ultra-lightweight robotic Gen3 arm (Kinova Robotics, Canada) as shown in Fig. 1. Kinova Gen3 is a robotic arm for compliant industrial application and safe human-robot collaboration. The maximum reachable distance of the manipulator is 902 mm with the maximum Cartesian translation speed being 40 cm/s. The mobile base is equipped with two pairs of Mecanum wheels, so it can undertake omnidirectional motion. It is noteworthy that the WMM system is controlled at the velocity level. Thus in this paper, the integral of the calculated joint acceleration was commanded to the robotic system. The control code was developed in C++, using the Eigen library [34] for algebraic computations. The experiments were performed utilizing the ROS environment [35] on a Intel(R) Xeon(R) CPU X5550 @ 2.67 GHz, with 16 GB of RAM.

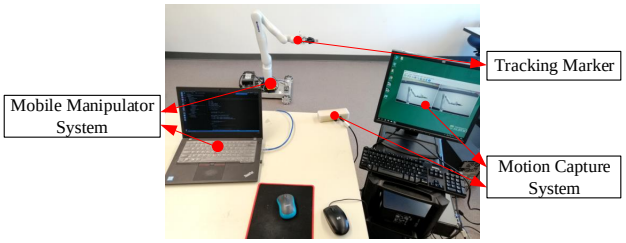

Figure 5: Experimental setup.

Fig. 5 presents the experimental setup, which consists of a WMM system (self-assembled) and a motion capture system (Claron Technology Inc., Canada) . The RMS value of the calibration accuracy of the motion capture system is 0.35 mm. It should be noted that the motion capture system is only used for obtaining the actual pose of the end-effector as ground truth to evaluate the kinematic accuracy of the proposed method and not employed in the motion planning system.

We select J as the WMM's Jacobian, as defined in (2). The generalized coordinate vector of the base (shown in Fig. 6) is defined as $q_b = [x_b, y_b, \theta_b]^{\mathrm{T}} \in \mathbb{R}^3$ and the velocity command vector of the wheels as $v_b = [\omega_{fl}, \omega_{fr}, \omega_{bl}, \omega_{br}]^{\mathrm{T}} \in \mathbb{R}^4$. The velocity transformation matrix $P(q_b) \in \mathbb{R}^{3\times4}$, which transfers the wheel velocity to the generalized base velocity, can be expressed as

$$P(q_b) = J_I J_V \quad (16)$$

with

$$J_I = \begin{bmatrix} \cos\theta_b & -\sin\theta_b & 0 \\ \sin\theta_b & \cos\theta_b & 0 \\ 0 & 0 & 1 \end{bmatrix},$$

and

$$J_V = \frac{R}{4}\begin{bmatrix} 1 & 1 & 1 & 1 \\ -1 & 1 & 1 & -1 \\ \frac{-1}{d_1+d_2} & \frac{1}{d_1+d_2} & \frac{-1}{d_1+d_2} & \frac{1}{d_1+d_2} \end{bmatrix}.$$

The variables θ_b, R, d_1, and d_2 are illustrated in Fig. 6.

The joint constraints of the WMM are listed in Table 1, where the units of angle, velocity, and acceleration for prismatic joints (the first and second joints) are m, m/s, and m/s^2;

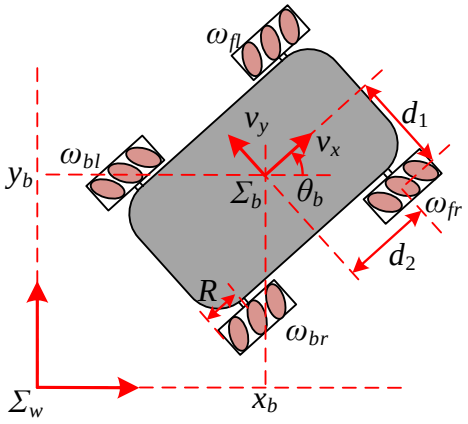

Figure 6: Description of the omnidirectional mobile base.

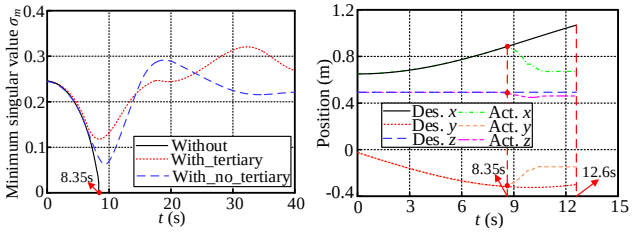

(a) Minimum singular value (b) Position of the end-effector

Figure 7: Results of the singularity avoidance experiment. The left plot presents the minimum singular value of the manipulator's Jacobian, and the right plot shows the end-effector position of the WMM using AMP method without singularity avoidance.

Table 1
Joint limits of WMM. The first three joints correspond to the mobile base and the rest seven joints to the manipulator.

Joint No.	Joint type	Angle	Velocity	Acceleration
1	Prismatic	$\pm\infty$	±0.25	±0.025
2	Prismatic	$\pm\infty$	±0.25	±0.025
3	Revolute	$\pm\infty$	±1.0	±1.5
4	Revolute	$\pm\infty$	±1.75	±3.0
5	Revolute	±2.2	±1.75	±3.0
6	Revolute	$\pm\infty$	±1.75	±3.0
7	Revolute	±2.5	±1.75	±3.0
8	Revolute	$\pm\infty$	±3.14	±5.0
9	Revolute	±2	±3.14	±5.0
10	Revolute	$\pm\infty$	±3.14	±5.0

and for revolute joints (the remaining eight joints) are rad, rad/s, and rad/s^2, respectively. The mobile base frame Σ_b is assumed to be the same as the world frame Σ_w at the start of the experiment. The initial joint position of the WMM is $q_0 = [0, 0, 0, 0, \pi/6, 0, \pi/2, 0, -\pi/6, 0]^{\mathrm{T}}$. Also, the start position of the end-effector in Σ_w is $[0.65, -0.0246, 0.4921]^{\mathrm{T}}$. In the following text, the initial state of the end-effector is denoted as x_0.

A video is attached with the manuscript to present the experiments in this section.

4.2. Experiments with and without Singularity Avoidance

The AMP method without singularity avoidance will often put the manipulator at a singular configuration. Although the employment of singularity avoidance will somewhat decrease the WMM's kinematic accuracy as it enables the mobile base, it is unavoidable. The AMP method and the modified AMP method (i.e., the AMP method with singularity avoidance) have been experimentally compared to verify the effectiveness of the latter. The end-effector acceleration $\ddot{x}$ in (5) is changed to $\ddot{x}_d + K_d(\dot{x}_d - \dot{x}) + K_p(x_d - x)$ to ensure that the trajectory tracking error converges to zero, where x_d is the desired end-effector trajectory, and K_d and K_p are two diagonal positive-definite matrices. The proof of this conclusion can be found in Appendix C. During the experiments in this section, only the end-effector's position is considered with $r = 3$. We define the desired end-effector trajectory as a circle with a radius of R, with the definition being $x_d(t) = x_0 + \left[-R(\cos(\pi/20t) - 1), -R\sin(\pi/20t), 0\right]^{\mathrm{T}}$. Here, we select the radius of the circle as $R = 0.25$ m. It should be noted that this radius is beyond the manipulator workspace (0.2 m) at its initial configuration. The closed-loop system parameters for the desired trajectory K_d and K_p are the same during the two experiments to indicate the fairness of the comparison, with $K_d = 10I_{3\times3}$ and $K_p = 20I_{3\times3}$. These two values are obtained by trial and error in this research; furthermore, an approach to optimize their values can be found in [36]. The other parameters are set as $\gamma_1 = 5$, $\gamma_2 = 0.5$, $\sigma_{m,min} = 0.15$. Line search techniques [37] are a preferable choice to determine the values of γ_1 and γ_2. The threshold value for singularity avoidance $\sigma_{m,min}$ is determined by trial and error to make the system put off the activation time of the mobile base as much as possible. It is noteworthy that these parameters are essential to complete the motion planner design to make the best use of the manipulator, but they do not play the major role in the proposed method. Fig. 7 presents the results during the experiment.

Fig. 7a shows the experimental results with singularity avoidance and without it. With the AMP method, the manipulator tried to complete the task alone and ultimately put itself at a singular configuration at about 8.35 s. This caused the system to be uncontrollable and made the task incomplete. However, with singularity avoidance, when the manipulator was near a singularity, the mobile base was activated and the manipulator could adjust its configuration to move away from it. Thus, the task could still be executed. The performance of the tertiary objective can be found by comparing the values of σ_m using tertiary objective and not using it. With the tertiary objective, the manipulator can have a better configuration to stay away from a singularity. Fig. 7b shows the end-effector's position when no singularity avoidance was adopted, the desired trajectory could not be tracked at about 8.35 s and significant kinematic errors started to emerge in all Cartesian directions.

The activation of the mobile base for singularity avoidance is a trade-off between the WMM's kinematic accuracy and the manipulator's singularity. The earlier the mobile base is employed, the farther the manipulator will be from the singularity, and the lower the WMM's kinematic accuracy will be. In this paper, the mobile base is enabled as late as possible to derive better kinematic accuracy, while the manipulator's singularity can still be avoided.

4.3. Experiments for Kinematic Accuracy Enhancement with Position Considered

The proposed motion planning approach can make the best use of the manipulator to execute tasks while keeping it from a singularity, and the mobile base is enabled only when the task cannot be executed by the manipulator alone or the manipulator is close to a singular configuration. With this method, the contribution of the base to the overall WMM motion is minimized, thus improving the kinematic precision of the WMM. The dimension of the Cartesian space of the WMM's end-effector is defined to be $r = 3$ as only its position is considered in this section.

The proposed AMP method is implemented to verify its efficiency compared with the traditional kinematic motion planning approach by following a predefined end-effector trajectory. The traditional motion planner in the experiment means using the pseudoinverse of the Jacobian $\boldsymbol{J}^{\dagger} = \boldsymbol{J}^{\mathrm{T}}(\boldsymbol{J}\boldsymbol{J}^{\mathrm{T}})^{-1}$ with considering manipulability enhancement for the manipulator in the null space [38]. At the acceleration level, this motion planner can be expressed as $\ddot{q} = \boldsymbol{J}^{\dagger}(\ddot{x} - \dot{\boldsymbol{J}}\dot{q}) + (\boldsymbol{I} - \boldsymbol{J}^{\dagger}\boldsymbol{J})\ddot{q}_A$, where $\ddot{q}_A$ is defined in (13). Two desired trajectories with the same definition as in Section 4.2 are provided, the first one is within the manipulator workspace and the second one is beyond it. The trajectory within the manipulator workspace is a circle with a radius of $R = 0.1$ m and the other one is a circle with a radius of $R = 0.25$ m. The motion planning parameters for the experiments in this section are the same as those in section 4.2. Figs. 8 and 9 show the experimental results within the manipulator workspace, and Figs. 10 and 11 present the results beyond the manipulator workspace. The average execution time for the proposed method and the traditional method were 14.8 ms and 12.4 ms in one loop, which demonstrated the desirable online performance of the proposed approach. It is worth mentioning that with the traditional method, the mobile base was always involved in the experiment and no joint saturation of the manipulator occurred. The actual position of the end-effector was obtained via the motion capture system to have ground-truth information. Table 2 contains the RMS value and duration time of the commanded base velocity in these two scenarios.

Fig. 8a shows that when the end-effector trajectory was within the manipulator workspace, with the proposed AMP method, there was only a small kinematic error. This is due to the fact that no motion was assigned to the base, as shown in the first column of Table 2. With no adaptive motion planning, some motions were imposed to the base, as shown in the second column of Table 2. Thus, the kinematic error was

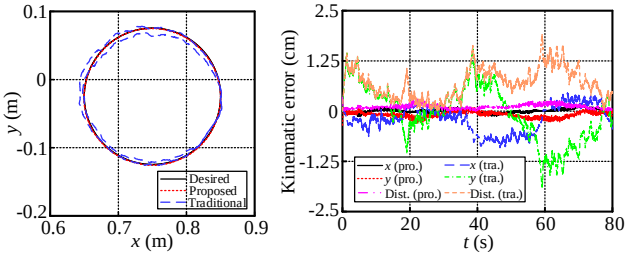

(a) End-effector trajectories (b) Kinematic errors

Figure 8: End-effector's kinematic accuracy with traditional and proposed methods (within manipulator workspace).

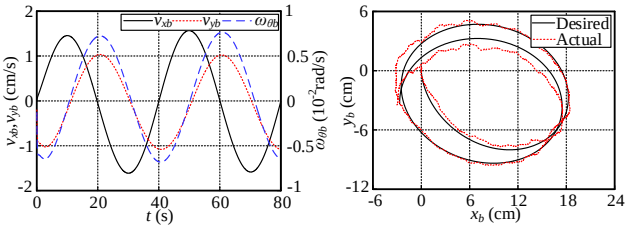

(a) Commanded velocities (b) Trajectories in $x - y$ plane

Figure 9: Motion of the mobile base with traditional method (within manipulator workspace).

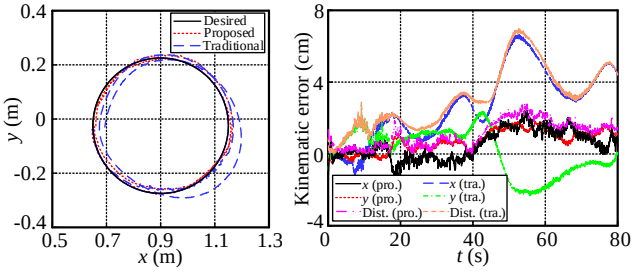

(a) End-effector trajectories (b) Kinematic errors

Figure 10: End-effector's kinematic accuracy with traditional and proposed methods (beyond manipulator workspace).

Table 2
RMS value and commanded duration of base velocity.

		Within		Beyond	
		Pro.	Tra.	Pro.	Tra.
x_b	RMS (cm/s)	0	1.10	1.58	2.77
	Duration (s)	0	80	12.08	80
y_b	RMS (cm/s)	0	0.75	0.24	1.86
	Duration (s)	0	80	12.08	80
θ_b	RMS (°/s)	0	0.287	0.241	0.739
	Duration (s)	0	80	12.08	80

much larger compared with the AMP scenario (as shown in Fig. 8b), with the maximum errors in x and y being 0.91 cm and 1.89 cm, respectively. Besides, the maximum distance between the desired and actual trajectories was improved from 1.91 cm to 0.45 cm with the proposed approach. Fig. 9 shows the motion of the mobile base with the tradi-

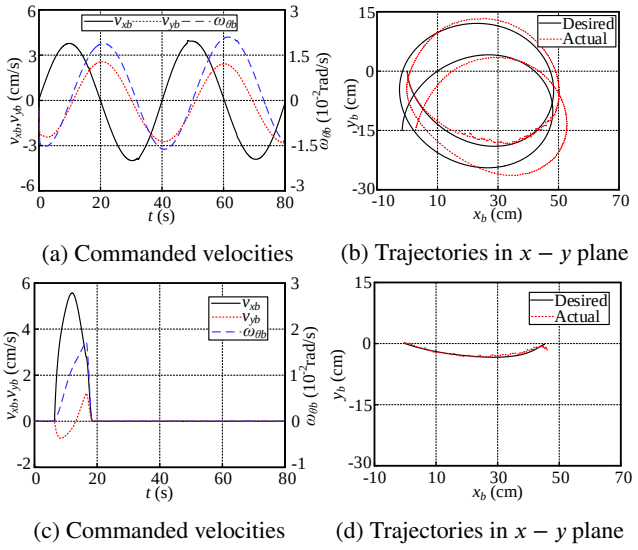

(a) Commanded velocities (b) Trajectories in $x-y$ plane

(c) Commanded velocities (d) Trajectories in $x-y$ plane

Figure 11: Motion of the mobile base with traditional and proposed methods (beyond manipulator workspace).

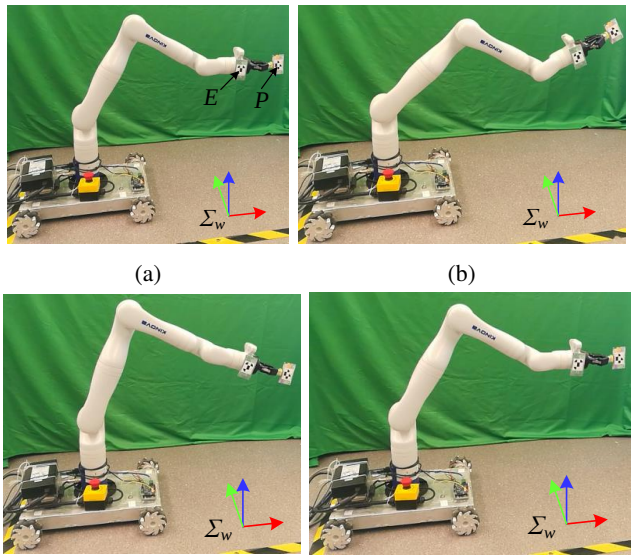

(a) (b)

(c) (d)

Figure 12: Screenshots of the experiment with the proposed approach. (a) shows the initial pose of the WMM, (b) shows the moment that the mobile base started to move, (c) shows the time that the mobile base ceased its motion, and (d) shows the final pose of the WMM during one period.

tional method, where v_{xb}, v_{yb}, $\omega_{\theta b}$ represent the commanded base velocities in x_b, y_b, and θ_b, respectively. The motion of the mobile base with the proposed method is not presented since no motion is distributed to it.

The last two columns of Table 2 show that when the desired end-effector trajectory was beyond the manipulator workspace, the mobile base was always forced to move. However, the base movement was much smaller if one adopted the proposed AMP method. The commanded duration time and RMS values of the base velocity in x_b, y_b, and θ_b represented 15.10%, 57.04%, 12.90%, and 32.61% of the commands without motion planning, respectively. Fig. 10 contains the end-effector's kinematic accuracy results. Fig. 10b shows that the maximum kinematic error in x was reduced from 6.65 cm to 2.44 cm, in y was reduced from 2.72 cm to 1.82 cm, and in distance of $x-y$ plane was decreased from 6.97 cm to 2.78 cm compared with no motion planning scenario.

Fig. 11 presents the motion of the mobile base when the desired end-effector trajectory was beyond the manipulator workspace with two different methods. Figs. 11a and 11b show that with the traditional method, the mobile base was consistently distributed with some motions. Thus, the end-effector's kinematic accuracy was low. The mobile base motion with the proposed method is shown in Figs. 11c and 11d. As shown in Fig. 11c, the base was activated at time 6.40 s. The manipulator regained enough manipulability at about 16.48 s. However, the base was not deactivated suddenly due to the implementation of the transition function (15); instead, it gradually stopped. Fig. 11d shows the desired and actual trajectories of the mobile base in the $x-y$ plane with the proposed method. We define the integral of the mobile base's kinematic error as $\frac{\int_{T_s}^{T_f}|e_{i_b}|dt}{T_f-T_s}$, where T_s and T_f represent the start time and final time of the base motion, and e_{i_b} denotes its kinematic error. With the traditional approach, the integral of the errors in x_b and y_b were 2.81 cm and 1.12 cm, respectively, while these values were decreased to 0.81 cm and 0.37 cm with the proposed approach. To sum up, the distributed motion to the mobile base was much less, and the WMM's kinematic accuracy was improved significantly with the proposed method.

4.4. Experiments for Kinematic Accuracy Enhancement with Pose Considered

The proposed AMP approach in enhancing the WMM's kinematic accuracy with the end-effector's pose considered is verified here. Thus the end-effector's Cartesian space dimension is selected as $r = 6$. The traditional motion planner utilized in this section is similar to the one in Section 4.3. In the experiments, the end-effector was planned to move in the x axis and rotate along the y axis of the world frame.

The desired pose of the end-effector is defined as $x_d(t) = x_0 + \left[0.15\sin(\pi/20t), 0, 0, 0, \pi/4\sin(\pi/20t), 0\right]^{\mathrm{T}}$. With this setting of the end-effector's pose, the mobile base was forced to move even using the proposed method. The closed-loop system parameters are chosen as $K_d = \mathrm{diag}(10, 10, 10, 3, 3, 3)$ and $K_p = \mathrm{diag}(20, 20, 20, 5, 5, 5)$. The remainder motion planning parameters are selected as $\gamma_1 = 5, \gamma_2 = 0.5, \sigma_{m,min} = 0.19$. Fig. 12 presents some screenshots of the experiments with the proposed method. The actual end-effector's position was obtained using the marker attached at point E via the motion capture system. Meanwhile, its orientation was acquired by calculating the angle between the marker pasted at point P and the desired position of point E.

Fig. 13 shows the end-effector's kinematic accuracy during the experiments. Fig. 14 presents the mobile base's

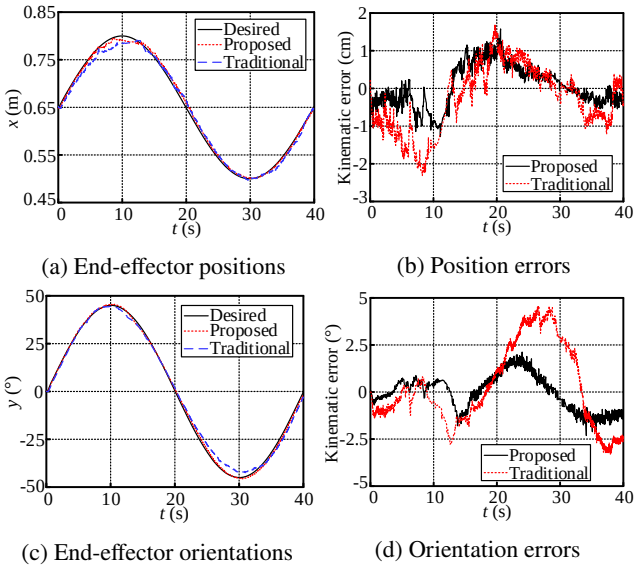

(a) End-effector positions (b) Position errors

(c) End-effector orientations (d) Orientation errors

Figure 13: End-effector's kinematic accuracy with its full pose considered.

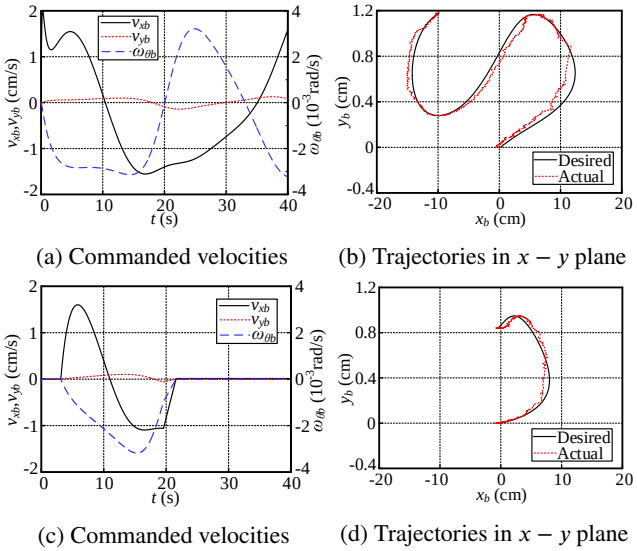

(a) Commanded velocities (b) Trajectories in $x-y$ plane

(c) Commanded velocities (d) Trajectories in $x-y$ plane

Figure 14: Motion of the mobile base with end-effector's full pose considered.

Table 3
RMS value and duration of commanded mobile base velocity.

	x_b		y_b		θ_b	
	RMS	Dura.	RMS	Dura.	RMS	Dura.
Pro.	0.67	18.48 s	0.044	18.48	0.08	18.48
Tra.	1.18	40 s	0.082	40	0.13	40

motion with the traditional and the proposed methods. The RMS value and duration of the commanded mobile base velocity in these two scenarios are displayed in Table 3. Here, the units of these variables are the same as the ones in Table 2.

As shown in Figs. 13b and 13d, the maximum kinematic error of the end-effector's x-axis position and y-axis orientation was improved from 2.31 cm and 4.58° to 1.58 cm and 2.32°, respectively, with the AMP approach. The precision difference was caused by the motion of the mobile base. When the traditional method was adopted, the mobile base was constantly activated (as shown in Fig. 14a and the second row of Table 3). In contrast, the mobile base moved for about 18.48 s of the entire 40 s with the proposed approach (as shown in Fig. 14c and the first row of Table 3), where the start time and final time of the mobile base motion were 3.1 s and 21.58 s. The RMS values of the commanded base velocity with the AMP method in x_b, y_b, and θ_b stood for 56.78%, 53.66%, and 61.54% of the commands without motion planning, respectively.

Figs. 14b and 14d present the mobile base's trajectories in the $x-y$ plane with the traditional method and the proposed approach, respectively. The motion range of the mobile base was much smaller with the proposed method than the conventional method. Furthermore, the integral of the mobile base's kinematic error was enhanced from 0.74 cm to 0.47 cm when the proposed method was adopted.

Although the kinematic accuracy of a WMM is enhanced with the proposed AMP method, there are still some challenges. For motion tracking, two things affect their accuracy (kinematic accuracy and dynamic accuracy) [39]. In this paper, we did not consider the dynamics of the robotic system and the transient errors of the motion capture system. The investigation of both the kinematic and dynamic accuracies remains for future research.

5. Conclusions

A new approach to enhance the kinematic accuracy of a wheeled mobile manipulator (WMM) was proposed considering the need for singularity avoidance. To improve the kinematic accuracy of the WMM, we presented an adaptive motion planning method to transfer more motions to the manipulator due to the low kinematic precision of the mobile base. Using the proposed motion planning method, the mobile base of the WMM was immobile until all the redundancy of the manipulator for the task was employed or the manipulator was close to a singularity. Only when the manipulator's remaining unsaturated joints were not enough for performing the task, would the motion planner assign some of the motions to the mobile base to execute. To avoid singularity, we adopted the task priority method to define manipulability enhancement as a tertiary task. In summary, when the primary task (kinematic accuracy enhancement) and the secondary task (adaptive motion planning) were resolved, the remaining DOFs could be used to keep the system away from the singularity (tertiary task). The proposed approach was designed at the acceleration level to avoid the discontinuity of the joint velocity due to the activation or termination of the mobile base.

The effectiveness of the proposed approach has been experimentally verified compared with a traditional method by following several predefined end-effector trajectories. When only the end-effector's position was considered, for the con-

dition that the desired end-effector trajectory was beyond the manipulator workspace, the maximum kinematic error of the end-effector was improved by 63.3% and 33.1% in x and y, respectively, and the motion time of the mobile base declined by 84.9%. When the end-effector's full pose was considered, its position kinematic error in x and orientation kinematic error along y were enhanced by 32.6% and 49.3%, respectively, and the motion duration of the mobile base was reduced by 53.8%.

In future works, we will establish the dynamic model of the WMM system and take both the motion planning and control of the robotic system into consideration to further enhance the motion accuracy of the system.

Acknowledgements

The authors gratefully acknowledge Teng Li for his assistance in the experiments.

A. Derivation of Joint Velocity for Singularity Avoidance

Define the partial derivative of J_m with respect to q_m as $\partial_q J$, and in the following expressions, the subscript m will be omitted for better readability (it is worth mentioning that q and J in the two Appendixes are only for the manipulator, not the entire WMM system). Specify $\Psi = JJ^{\mathrm{T}}$, the singularity avoidance velocity for the manipulator can be expressed as

$$\begin{aligned}\nabla_q H &= \nabla_q \det(\Psi) = \det(\Psi)\mathrm{tr}\left[\Psi^{-1}(\partial_q \Psi)\right] \\ &= \det(\Psi)\mathrm{tr}\left[\Psi^{-1}(\partial_q J J^{\mathrm{T}} + J\partial_q^{\mathrm{T}} J)\right].\end{aligned} \tag{17}$$

B. Derivation of Joint Acceleration for Singularity Avoidance

Consider two arbitrary manipulator joint angles p and q, define the second order derivative of J_m first by p and second by q as $\partial_{pq} J$. First, the second order derivative of Ψ by joint position is derived as

$$\begin{aligned}\partial_{pq}\Psi &= \partial_{pq}(JJ^{\mathrm{T}}) = \partial_q[\partial_p(JJ^{\mathrm{T}})] = \partial_q[\partial_p J\, J^{\mathrm{T}} + J\partial_p^{\mathrm{T}} J] \\ &= \partial_{pq} JJ^{\mathrm{T}} + \partial_p J\partial_q^{\mathrm{T}} J + \partial_q J\partial_p^{\mathrm{T}} J + J\partial_{pq}^{\mathrm{T}} J.\end{aligned} \tag{18}$$

According to (17), the second order derivative of H with respect to joint position can be expressed as

$$\begin{aligned}&\partial_{pq} H = \partial_{pq}\det(\Psi) = \partial_q(\det(\Psi))\mathrm{tr}(\Psi^{-1}\partial_p\Psi) + \\ &\det(\Psi)\mathrm{tr}(\partial_q(\Psi^{-1}\partial_p\Psi)) = \det(\Psi)\mathrm{tr}(\Psi^{-1}\partial_q\Psi)\mathrm{tr}(\Psi^{-1}\partial_p\Psi) + \\ &\det(\Psi)\mathrm{tr}\left(\partial_q(\Psi^{-1})\partial_p\Psi\right) + \det(\Psi)\mathrm{tr}(\Psi^{-1}\partial_{pq}\Psi).\end{aligned} \tag{19}$$

Then, with the fact that $\partial_q(\Psi^{-1}) = -\Psi^{-1}(\partial_q\Psi)\Psi^{-1}$, we can simplify (19) by factoring out $\det(\Psi)$ as

$$\begin{aligned}&\partial_{pq} H = \det\Psi\left[\mathrm{tr}(\Psi^{-1}\partial_q\Psi)\mathrm{tr}(\Psi^{-1}\partial_p\Psi) - \right. \\ &\left.\mathrm{tr}(\Psi^{-1}\partial_q\Psi\Psi^{-1}\partial_p\Psi) + \mathrm{tr}(\Psi^{-1}\partial_{pq}\Psi)\right].\end{aligned} \tag{20}$$

For the general case when $p = q$ represents the manipulator joint position vector, the singularity avoidance acceleration can be obtained as

$$\begin{aligned}&\nabla_q^2 H = \det\Psi\left[\left(\mathrm{tr}(\Psi^{-1}\partial_q\Psi)\right)^2 - \right. \\ &\left.\mathrm{tr}(\Psi^{-1}\partial_q\Psi\Psi^{-1}\partial_q\Psi) + \mathrm{tr}(\Psi^{-1}\partial_{qq}\Psi)\right].\end{aligned} \tag{21}$$

C. End-Effector's Trajectory Convergence Proof via Acceleration Command

At the acceleration level, the WMM's kinematic model is shown in (5) as

$$\ddot{q} = J^{\dagger}(\ddot{x} - \dot{J}\dot{q}) + (I - J^{\dagger}J)\ddot{q}_N. \tag{22}$$

The commanded joint acceleration is calculated as

$$\ddot{q} = J^{\dagger}(\ddot{x}_d + K_d(\dot{x}_d - \dot{x}) + K_p(x_d - x) - \dot{J}\dot{q}) + (I - J^{\dagger}J)\ddot{q}_N. \tag{23}$$

Combining (22) and (23), we can derive

$$(\ddot{x}_d - \ddot{x}) + K_d(\dot{x}_d - \dot{x}) + K_p(x_d - x) = 0. \tag{24}$$

Define the task-space position tracking error as $e = x_d - x$, we can obtain

$$\ddot{e} + K_d\dot{e} + K_p e = 0. \tag{25}$$

Consider the Lyapunov function candidate

$$V = \frac{1}{2}\dot{e}^{\mathrm{T}}\dot{e} + \frac{1}{2}e^{\mathrm{T}}K_p e, \tag{26}$$

the time derivative of V along the trajectory of the closed-loop system (25) is

$$\dot{V} = \dot{e}^{\mathrm{T}}\ddot{e} + e^{\mathrm{T}}K_p\dot{e} = -\dot{e}^{\mathrm{T}}K_d\dot{e} \leqslant 0. \tag{27}$$

Since V is positive definite and $\dot{V}$ is negative semi-definite, the closed-loop system (25) is stable. If $\dot{V} \equiv 0$, then, $\dot{e} \equiv 0$; thus, $\ddot{e} \equiv 0$. Refer to (25), we can derive $e = x_d - x = 0$. According to LaSalle's theorem [40], $(e, \dot{e}) = (0, 0)$ is the asymptotically stable equilibrium point of (25). Thus, $\lim_{t\to\infty}(x \to x_d)$.

CRediT authorship contribution statement

Hongjun Xing: Conceptualization, Methodology, Writing - original draft, Writing - review & editing, Validation. **Ali Torabi:** Conceptualization, Methodology, Supervision, Writing - review & editing, Validation. **Liang Ding:** Resources, Supervision, Writing - review & editing. **Haibo Gao:** Resources, Supervision. **Weihua Li:** Supervision, Validation. **Mahdi Tavakoli:** Resources, Supervision, Funding acquisition, Project administration.

References

[1] S. Ahmad, H. Zhang, G. Liu, Multiple working mode control of door-opening with a mobile modular and reconfigurable robot, IEEE/ASME Transactions on Mechatronics 18 (3) (2012) 833–844.

[2] H. Xing, K. Xia, L. Ding, H. Gao, G. Liu, Z. Deng, Unknown geometrical constraints estimation and trajectory planning for robotic door-opening task with visual teleoperation assists, Assembly Automation 39 (3) (2019) 479–488.

[3] S. R. Ahmadzadeh, P. Kormushev, R. S. Jamisola, D. G. Caldwell, Learning reactive robot behavior for autonomous valve turning, in: IEEE-RAS International Conference on Humanoid Robots, 2014, pp. 366–373.

[4] Z. Li, S. S. Ge, Z. Wang, Robust adaptive control of coordinated multiple mobile manipulators, Mechatronics 18 (5-6) (2008) 239–250.

[5] D. Sun, Q. Liao, A. Kiselev, T. Stoyanov, A. Loutfi, Shared mixed reality-bilateral telerobotic system, Robotics and Autonomous Systems 134 (2020) 103648.

[6] X. Zhang, M. Li, J. H. Lim, Y. Weng, Y. W. D. Tay, H. Pham, Q.-C. Pham, Large-scale 3d printing by a team of mobile robots, Automation in Construction 95 (2018) 98–106.

[7] Y. Jia, N. Xi, Y. Cheng, S. Liang, Coordinated motion control of a nonholonomic mobile manipulator for accurate motion tracking, in: IEEE/RSJ International Conference on Intelligent Robots and Systems, 2014, pp. 1635–1640.

[8] A. Torabi, K. Zareinia, G. R. Sutherland, M. Tavakoli, Dynamic reconfiguration of redundant haptic interfaces for rendering soft and hard contacts, IEEE Transactions on Haptics (2020).

[9] I.-L. G. Borlaug, K. Y. Pettersen, J. T. Gravdahl, Combined kinematic and dynamic control of vehicle-manipulator systems, Mechatronics 69 (2020) 102380.

[10] J. Sverdrup-Thygeson, S. Moe, K. Y. Pettersen, J. T. Gravdahl, Kinematic singularity avoidance for robot manipulators using set-based manipulability tasks, in: IEEE Conference on Control Technology and Applications, 2017, pp. 142–149.

[11] H. Zhang, Y. Jia, N. Xi, Sensor-based redundancy resolution for a nonholonomic mobile manipulator, in: IEEE/RSJ International Conference on Intelligent Robots and Systems, 2012, pp. 5327–5332.

[12] T. Yoshikawa, Manipulability of robotic mechanisms, The International Journal of Robotics Research 4 (2) (1985) 3–9.

[13] A. Torabi, M. Khadem, K. Zareinia, G. R. Sutherland, M. Tavakoli, Application of a redundant haptic interface in enhancing soft-tissue stiffness discrimination, IEEE Robotics and Automation Letters 4 (2) (2019) 1037–1044.

[14] W. Li, Z. Liu, H. Gao, X. Zhang, M. Tavakoli, Stable kinematic teleoperation of wheeled mobile robots with slippage using time-domain passivity control, Mechatronics 39 (2016) 196–203.

[15] Z. Song, H. Ren, J. Zhang, S. S. Ge, Kinematic analysis and motion control of wheeled mobile robots in cylindrical workspaces, IEEE Transactions on Automation Science and Engineering 13 (2) (2015) 1207–1214.

[16] D. H. Shin, B. S. Hamner, S. Singh, M. Hwangbo, Motion planning for a mobile manipulator with imprecise locomotion, in: IEEE/RSJ International Conference on Intelligent Robots and Systems, 2003, pp. 847–853.

[17] E. Papadopoulos, J. Poulakakis, Planning and model-based control for mobile manipulators, in: IEEE/RSJ International Conference on Intelligent Robots and Systems, 2000, pp. 1810–1815.

[18] K. Nagatani, T. Hirayama, A. Gofuku, Y. Tanaka, Motion planning for mobile manipulator with keeping manipulability, in: IEEE/RSJ International Conference on Intelligent Robots and Systems, 2002, pp. 1663–1668.

[19] H. Xing, A. Torabi, L. Ding, H. Gao, Z. Deng, M. Tavakoli, Enhancement of force exertion capability of a mobile manipulator by kinematic reconfiguration, IEEE Robotics and Automation Letters 5 (4) (2020) 5842–5849.

[20] G. Antonelli, S. Chiaverini, Fuzzy redundancy resolution and motion coordination for underwater vehicle-manipulator systems, IEEE Transactions on Fuzzy Systems 11 (1) (2003) 109–120.

[21] F.-T. Cheng, T.-H. Chen, Y.-Y. Sun, Resolving manipulator redundancy under inequality constraints, IEEE Transactions on Robotics and Automation 10 (1) (1994) 65–71.

[22] A. D. Prete, Joint position and velocity bounds in discrete-time acceleration/torque control of robot manipulators, IEEE Robotics and Automation Letters 3 (1) (2018) 281–288.

[23] M. Giftthaler, F. Farshidian, T. Sandy, L. Stadelmann, J. Buchli, Efficient kinematic planning for mobile manipulators with non-holonomic constraints using optimal control, in: IEEE International Conference on Robotics and Automation, 2017, pp. 3411–3417.

[24] A. Karami, H. Sadeghian, M. Keshmiri, G. Oriolo, Hierarchical tracking task control in redundant manipulators with compliance control in the null-space, Mechatronics 55 (2018) 171–179.

[25] O. Kanoun, F. Lamiraux, P.-B. Wieber, Kinematic control of redundant manipulators: Generalizing the task-priority framework to inequality task, IEEE Transactions on Robotics 27 (4) (2011) 785–792.

[26] A. Escande, N. Mansard, P.-B. Wieber, Hierarchical quadratic programming: Fast online humanoid-robot motion generation, The International Journal of Robotics Research 33 (7) (2014) 1006–1028.

[27] F. Flacco, A. De Luca, O. Khatib, Control of redundant robots under hard joint constraints: Saturation in the null space, IEEE Transactions on Robotics 31 (3) (2015) 637–654.

[28] A. De Luca, G. Oriolo, P. R. Giordano, Kinematic modeling and redundancy resolution for nonholonomic mobile manipulators, in: IEEE International Conference on Robotics and Automation, 2006, pp. 1867–1873.

[29] Y. Dai, S. Yu, Y. Yan, X. Yu, An ekf-based fast tube mpc scheme for moving target tracking of a redundant underwater vehicle-manipulator system, IEEE/ASME Transactions on Mechatronics 24 (6) (2019) 2803–2814.

[30] H. Xing, A. Torabi, L. Ding, H. Gao, Z. Deng, V. K. Mushahwar, M. Tavakoli, An admittance-controlled wheeled mobile manipulator for mobility assistance: Human–robot interaction estimation and redundancy resolution for enhanced force exertion ability, Mechatronics 74 (2021) 102497.

[31] B. Siciliano, Kinematic control of redundant robot manipulators: A tutorial, Journal of Intelligent and Robotic Systems 3 (3) (1990) 201–212.

[32] F. Flacco, A. De Luca, O. Khatib, Motion control of redundant robots under joint constraints: Saturation in the null space, in: IEEE International Conference on Robotics and Automation, 2012, pp. 285–292.

[33] S. Chiaverini, Singularity-robust task-priority redundancy resolution for real-time kinematic control of robot manipulators, IEEE Transactions on Robotics and Automation 13 (3) (1997) 398–410.

[34] G. Guennebaud, B. Jacob, et al., Eigen v3, URL: http://eigen. tuxfamily. org (2010).

[35] M. Quigley, K. Conley, B. Gerkey, J. Faust, T. Foote, J. Leibs, R. Wheeler, A. Y. Ng, ROS: An open-source robot operating system, in: ICRA workshop on open source software, Kobe, Japan, 2009.

[36] J.-J. Slotine, L. Weiping, Adaptive manipulator control: A case study, IEEE Transactions on Automatic Control 33 (11) (1988) 995–1003.

[37] D. G. Luenberger, Y. Ye, Linear and Nonlinear Programming, Springer, 1984.

[38] F. Vigoriti, F. Ruggiero, V. Lippiello, L. Villani, Control of redundant robot arms with null-space compliance and singularity-free orientation representation, Robotics and Autonomous Systems 100 (2018) 186–193.

[39] L. Ding, S. Li, H. Gao, C. Chen, Z. Deng, Adaptive partial reinforcement learning neural network-based tracking control for wheeled mobile robotic systems, IEEE Transactions on Systems, Man, and Cybernetics: Systems 50 (7) (2020) 2512–2523.

[40] R. Kelly, Comments on "adaptive PD controller for robot manipulators", IEEE Transactions on Robotics and Automation 9 (1) (1993) 117–119.

Hongjun Xing was born in 1992. He received the B.Sc. and M.Sc. degrees from the Harbin Institute of Technology, China, in 2015 and 2017, respectively, where he is currently pursuing the Ph.D. degree with the School of Mechatronics Engineering. From 2019 to 2021, he was a visiting student with the University of Alberta, Edmonton, AB, Canada.

His research interests include dynamic modeling, tele-robotics, and compliance control.

Ali Torabi received the BSc degree in mechanical engineering from Amirkabir University of Technology (Tehran Polytechnic) in 2010 and the MSc degree in mechanical engineering from Sharif University of Technology in 2013. He is currently pursuing a Ph.D. in Electrical Engineering at University of Alberta.

His research interests are control engineering, robotic and medical teleoperation systems.

Liang Ding was born in 1980. He received the Ph.D. degree in mechanical engineering from the Harbin Institute of Technology, Harbin, China, in 2009.

He is currently a Professor with the State Key Laboratory of Robotics and System, Harbin Institute of Technology. His current research interests include field and aerospace robotics and control.

Haibo Gao was born in 1970. He received the Ph.D. degree in mechanical design and theory from the Harbin Institute of Technology, Harbin, China, in 2004.

He is currently a Professor with the State Key Laboratory of Robotics and System, Harbin Institute of Technology. His current research interests include specialized and aerospace robotics and mechanisms.

Weihua Li received the M.Sc. and Ph.D. degrees in manufacturing engineering of aerospace vehicle from the Harbin Institute of Technology, Harbin, China, in 2011 and 2016, respectively.

He is currently an Assistant Professor with the School of Automotive Engineering, Harbin Institute of Technology (Weihai). His current research interests include the dynamics, simulation, and teleoperation of wheeled mobile robots.

Mahdi Tavakoli is a Professor in the Department of Electrical and Computer Engineering, University of Alberta, Canada. He received his BSc and MSc degrees in Electrical Engineering from Ferdowsi University and K.N. Toosi University, Iran, in 1996 and 1999, respectively. He received his PhD degree in Electrical and Computer Engineering from the University of Western Ontario, Canada, in 2005.

In 2006, he was a post-doctoral researcher at Canadian Surgical Technologies and Advanced Robotics (CSTAR), Canada. In 2007-2008, he was an NSERC Post-Doctoral Fellow at Harvard University, USA. Dr. Tavakoli's research interests broadly involve the areas of robotics and systems control. Dr. Tavakoli is the lead author of Haptics for Teleoperated Surgical Robotic Systems (World Scientific, 2008). He is an Associate Editor for IEEE/ASME Transactions on Mechatronics, Journal of Medical Robotics Research, IET Control Theory & Applications, and Mechatronics.